ON DETERMINISTIC APPROXIMATION OF THE BOLTZMANN EQUATION IN A BOUNDED DOMAIN

FRANCIS FILBET

Abstract. In this paper we present several numerical results performed with a fully deterministic scheme to discretize the Boltzmann equation of rarefied gas dynamics in a bounded domain for multi-scale problems. Periodic, specular reflection and diffusive boundary conditions are discussed and investigated numerically. The collision operator is treated by a Fourier approximation of the collision integral, which guarantees spectral accuracy in velocity with a computational cost of $M\,N\,\log(N)$, where N is the number of degree of freedom in velocity space and M represents the the number of discrete angles of the collision kernel. This algorithm is coupled with a second order finite volume scheme in space and a time discretization allowing to deal for rarefied regimes as well as their hydrodynamic limit. Our numerical results show that the proposed approach significantly improves the near-wall non stationary flow accuracy of standard numerical methods over a wide range of Knudsen numbers. In particular when the solution to the Boltzmann equation is closed to the local equilibrium and for slow motion flows.

Keywords. Boltzmann equation; spectral methods; asymptotic stability; boundary values problem.

AMS Subject Classification. 65N08, 65N35, 82C40.

Contents

1. Introduction

The construction of numerical methods to approximate the solution to the Boltzmann equation is an important problem for non stationary and rarefied flows. The difficulties related to the structure of the Boltzmann equation make it extremely difficult in most physically relevant situations. For such reasons realistic numerical simulations are based on Monte-Carlo techniques. The most famous examples are the Direct Simulation Monte-Carlo (DSMC) methods by Bird [1] and by Nanbu [28]. These methods can successfully simulate high speed transition flows. In contrast, the flow encountered in micro-scale and nano-scale systems typically involve low Mach Numbers and low Knudsen numbers. Under these conditions, DSMC approach is not computationally efficient

The author is partially supported by the European Research Council ERC Starting Grant 2009, project 239983-*NuSiKiMo*.

due to the requirement to perform large amounts of data sampling in order to reduce the statistical noise. This inconvenient offer a wide range of applications to fully deterministic methods for which there is no fluctuation. Numerical methods based on the use of spectral techniques in the velocity space has been developed in [30, 31, 33], inspired by previous works on the use of Fourier transform techniques for the Boltzmann equation (see [2] for instance). The spectral method has been applied later to non homogeneous situations [16, 19], to the Landau equation [15, 32], where fast algorithms can be readily derived, and to the case of granular gases [27, 17]. In [26], C. Mouhot & L. Pareschi proposed a fast spectral method was proposed on the basis of the previous spectral method together with a suitable semi-discretization of the collision operator. This method permits to reduce the computational cost from $O(N^2)$, where N denotes the total number of grid points in velocity space to $O(M\,N\log_2 N)$, without loosing the spectral accuracy, where M is an additional numerical parameter representing the number of discrete angles [26, 18]. The principles and basic features of this method will be presented in the next sections. Finally let us mention that A. Bobylev & S. Rjasanow [4, 5] have also constructed fast algorithms based on a Fourier transform approximation of the distribution function.

The goal of this paper is to apply the fast spectral method already developed in [18] together with an efficient time discretization technique [20] for problems where boundary conditions play a significant role in the long time asymptotic behavior of the solution to the Boltzmann equation. In particular, for low speed and low Knudsen flows for which DSMC methods are unsuitable. The plan of the paper is the following. In the next sections we recall the Boltzmann equation in a bounded domain and describe different types of boundary conditions. Therefore, we present the main ingredients for the approximation of the Boltzmann equation : a Fourier-Galerkin method for the Boltzmann operator [31, 16, 19, 26, 18], a second order finite volume scheme for the transport [14] and finally a stable scheme for the time discretization allowing to treat a wide range of regimes (from rarefied to hydrodynamic) [20]. Then, Section 5 is devoted to numerical simulations for one and two dimensional, time dependent and stationary problems. Finally, in the last section we draw conclusions.

2. The Boltzmann equation in a bounded domain

The Boltzmann equation describes the behavior of a dilute gas of particles when the only interactions taken into account are binary elastic collisions. It reads for $x \in \Omega \subset \mathbb{R}^d$, $v \in \mathbb{R}^d$ ($d \geq 2$):

$$\frac{\partial f}{\partial t} + v \cdot \nabla_x f = \frac{1}{\varepsilon}\mathcal{Q}(f), \tag{2.1}$$

where $f := f(t,x,v)$ is the time-dependent particles distribution function in the phase space. The parameter $\varepsilon > 0$ is the dimensionless Knudsen number defined as the ratio of the mean free path over a typical length scale such as the size of the spatial domain, which measures if the gas is rarefied. The Boltzmann collision operator $\mathcal{Q}$ is a quadratic operator local in (t,x). The time t and position x only act as parameters in $\mathcal{Q}$ and therefore will be omitted in its description

$$\mathcal{Q}(f)(v) = \int_{v_\star\in\mathbb{R}^d}\int_{\sigma\in\mathbb{S}^{d-1}} B(|v-v_\star|,\cos\theta)\,\left(f'_\star f' - f_\star f\right)\,d\sigma\,dv_\star. \tag{2.2}$$

We used the shorthand $f = f(v)$, $f_\star = f(v_\star)$, $f' = f(v')$, $f'_\star = f(v'_\star)$. The velocities of the colliding pairs $(v, v_\star)$ and $(v', v'_\star)$ are related by

$$\left\{\begin{array}{l} v' = v - \dfrac{1}{2}\big((v-v_\star) - |v-v_\star|\,\sigma\big), \\[2ex] v'_\star = v - \dfrac{1}{2}\big((v-v_\star) + |v-v_\star|\,\sigma\big), \end{array}\right.$$

with $\sigma \in \mathbb{S}^{d-1}$. The collision kernel B is a non-negative function which by physical arguments of invariance only depends on $|v - v_\star|$ and $\cos\theta = u \cdot \sigma$, where $u = (v - v_\star)$ and $\hat{u} = u/|u|$ is the normalized relative velocity. In this work we are concerned with *short-range interaction* models and we assume that B is locally integrable. These assumptions are satisfied for the so-called *hard spheres model* $B(u, \cos\theta) = |u|$, and it is known as *Grad's angular cutoff assumption* when it is (artificially) extended to interactions deriving from a power-law potentials. As an important benchmark model for the numerical simulation we therefore consider in this paper *variable hard spheres model* (VHS), which writes

$$B(u, \cos\theta) = C_\gamma \, |u|^\gamma, \tag{2.3}$$

for some $\gamma \in (0, 1]$ and a constant $C_\gamma > 0$.

Boltzmann's collision operator has the fundamental properties of conserving mass, momentum and energy

$$\int_{\mathbb{R}^d} \mathcal{Q}(f) \begin{pmatrix} 1 \\ v \\ |v|^2 \end{pmatrix} dv = 0,$$

and it satisfies well-known Boltzmann's H theorem

$$\frac{dH}{dt}(t) := -\frac{d}{dt}\int_{\mathbb{R}^d} f \log f \, dv = -\int_{\mathbb{R}^d} \mathcal{Q}(f)\log(f)\, dv \geq 0,$$

where the functional H is called the *entropy* of the solution. Boltzmann's H theorem implies that any equilibrium distribution function, *i.e.*, any function which is a maximum of the entropy, has the form of a locally Maxwellian distribution

$$\mathcal{M}[\rho, u, T](v) \;=\; \frac{\rho}{(2\,\pi\, k_B\, T)^{d/2}} \exp\left(-\frac{|u - v|^2}{2\, k_B\, T}\right),$$

where k_B is the Boltzmann constant, ρ, u, T are the *density*, *macroscopic velocity* and *temperature* of the gas, defined by

$$\rho = \int_{\mathbb{R}^d} f(v)\, dv, \quad u = \frac{1}{\rho}\int_{\mathbb{R}^d} v\, f(v)\, dv, \quad T = \frac{1}{d\rho}\int_{\mathbb{R}^d} |u - v|^2\, f(v)\, dv. \tag{2.4}$$

For further details on the physical background and derivation of the Boltzmann equation we refer to Cercignani, Illner, Pulvirenti [9] and Villani [40].

In order to define completely the mathematical problem for equation (2.1) suitable boundary conditions on $\partial\Omega$ should be considered. The most simple model for these is due to Maxwell [25], in which it is assumed that the fraction $(1-\alpha)$ of the emerging particles has been reflected elastically at the wall, whereas the remaining fraction α is thermalized and leaves the wall in a Maxwellian distribution. The parameter α is called accommodation coefficient [8].

More precisely, we consider equation (2.1) supplemented with the following boundary conditions for $x \in \partial\Omega$. The smooth boundary $\partial\Omega$ is assumed to have a unit outer normal $n(x)$ at every $x \in \partial\Omega$ and for $v \cdot n(x) \geq 0$, we assume that at the solid boundary a fraction α of particles is absorbed by the wall and then re-emitted with the velocities corresponding to those in a still gas at the temperature of the solid wall, while the remaining portion $(1 - \alpha)$ is perfectly reflected. This is equivalent to impose for the ingoing velocities

$$f(t, x, v) \;=\; (1 - \alpha)\, \mathcal{R}f(t, x, v) \;+\; \alpha\, \mathcal{M}\, f(t, x, v), \quad x \in \partial\Omega, \quad v \cdot n(x) \geq 0, \tag{2.5}$$

with $0 \leq \alpha \leq 1$ and

$$\begin{cases} \mathcal{R}f(t, x, v) &= f(t, x, v \,-\, 2\,(n(x) \cdot v)\, n(x)), \\ \\ \mathcal{M}f(t, x, v) &= \mu(t, x)\; f_w(v). \end{cases} \tag{2.6}$$

If we denote by k_B the Boltzmann's constant and by T_w the temperature of the solid boundary, f_w is given by

$$f_w(v) := \exp\left(-\frac{v^2}{2k_BT_w}\right),$$

and the value of $\mu(t,x)$ is determined by mass conservation at the surface of the wall for any $t \in \mathcal{R}^+$ and $x \in \partial\Omega$

$$\mu(t,x) \int_{v\cdot n(x)\geq 0} f_w(v)\, v\cdot n(x)\, dv = -\int_{v\cdot n(x)<0} f(t,x,v)\, v\cdot n(x)\, dv. \tag{2.7}$$

Hence, we have

Proposition 2.1. *Assume that f is a smooth solution to the Boltzmann equation (2.1) with boundary conditions (2.5)-(2.7). Then we have for any $x \in \partial\Omega$*

$$\begin{cases} \displaystyle\int_{v\cdot n(x)\geq 0} \mathcal{R}f(t,x,v)\, v\cdot n(x)\, dv = -\int_{v\cdot n(x)<0} f(t,x,v)\, v\cdot n(x)\, dv, \\ \displaystyle\int_{v\cdot n(x)\geq 0} \mathcal{R}f(t,x,v)\, v\cdot \tau(x)\, dv = +\int_{v\cdot n(x)<0} f(t,x,v)\, v\cdot \tau(x)\, dv, \end{cases} \tag{2.8}$$

where $\tau(x)$ belongs to the hyperplane orthogonal to $n(x)$, and

$$\int_{v\cdot n(x)\geq 0} \mathcal{M}f(t,x,v)\, v\cdot n(x)\, dv = -\int_{v\cdot n(x)<0} f(t,x,v)\, v\cdot n(x)\, dv. \tag{2.9}$$

Both equalities (2.8) and (2.9)guarantee the global conservation of mass.

Proof. First the equality (2.9) is straightforward by construction of the constant $\mu(t,x)$.

Then, to prove (2.8) for any $x \in \partial\Omega$, we multiply $\mathcal{R}f(t,x,f)$ by a function $\eta(v)$ in (2.6) and integrate on the set $\{v \in \mathbb{R}^d,\ (v\cdot n(x) \geq 0\}$. Applying the change of variable $v^* = v - 2(v\cdot n(x))\, n(x)$, it yields

$$\int_{v\cdot n(x)\geq 0} \mathcal{R}f(t,x,v)\, \eta(v)\, dv = \int_{v^*\cdot n(x)\leq 0} f(t,x,v^*)\, \eta\left(v^* - 2(v^*\cdot n(x))\, n(x)\right)\, dv^*.$$

Taking respectively $\eta(v) = v\cdot n(x)$ and $\eta(v) = v\cdot\tau(x)$ we get the result. □

3. General framework for the discretization of the Boltzmann operator

We consider the spatially homogeneous Boltzmann operator written in the following general form

$$\mathcal{Q}(f) = \int_{\mathcal{C}} \mathcal{B}(y)\left[f'f'_\star - f_\star f\right] dy, \quad v \in \mathbb{R}^d, \tag{3.1}$$

with

$$v' = v + \Theta'(y), \qquad v'_\star = v + \Theta'_\star(y), \qquad v_\star = v + \Theta_\star(y).$$

In the equations above, $\mathcal{C}$ is some given (unbounded) domain for y, and Θ, Θ', $\Theta'_\star$ are suitable functions, to be defined later. This general framework emphasizes the translation invariance property of the collision operator, which is crucial for the spectral methods. We will be more precise in the next paragraphs for some changes of variables allowing to reduce the classical operator (2.2) to the form (3.1).

In this section we remind the basic principles leading to Fourier-Galerkin approximation of the Boltzmann operator, the method is based on the following three steps:

- **1)** periodized truncations of the Boltzmann collision operator $\mathcal{Q}(f)$,
- **2)** expansion of the distribution function in a truncated Fourier series of degree $N = (n,\dots,n) \in \mathbb{N}^d$,

3) projection of the quadratic operator in the set of trigonometric polynomial of degree N.

3.1. **Periodized truncations of the Boltzmann collision operator.** Any deterministic numerical method requires to work in a *bounded* velocity space. Here, the idea only consists in adding some non physical binary collisions by *periodizing* the function and the collision operator. This implies the loss of some local invariants (some non physical collisions are added). Thus the scheme is not conservative anymore, although it still preserves the mass if the periodization is done carefully. However in this way the structural properties of the collision operator are maintained and thus they can be exploited to derive fast algorithms. This periodization is the basis of spectral methods and we shall discuss below this non physical truncation (associated with limit conditions) of this velocity space.

Let us consider the space homogeneous Boltzmann equation in a bounded domain in velocity $\mathcal{D}_L = [-L, L]^d$ with $0 < L < \infty$. We truncate the integration in y and z in (3.1) since periodization would yield infinite result if not: we set y and z to belong to some truncated domain $\mathcal{C}_R \subset \mathcal{C}$ (the parameter R refers to its size and will be defined later).

Then the *truncated* collision operator reads

$$\mathcal{Q}^R(f) = \int_{\mathcal{C}_R} \mathcal{B}(y) \left(f'_\star f' \, - \, f_\star f \right) dy, \tag{3.2}$$

for $v \in \mathcal{D}_L$ (the expression for $v \in \mathbb{R}^d$ is deduced by periodization). By making some changes of variable on v, one can easily prove for the two choices of variables y of the next subsections, that for any function φ periodic on $\mathcal{D}_L$ the following weak form is satisfied:

$$\int_{\mathcal{D}_L} \mathcal{Q}^R(f)\, \varphi(v)\, dv = \frac{1}{4} \int_{\mathcal{D}_L} \int_{\mathcal{C}_R} \mathcal{B}(y)\, f_\star f \, \left(\varphi'_\star + \varphi' - \varphi_\star - \varphi \right) \, dy\, dv. \tag{3.3}$$

Now, we use the representation $\mathcal{Q}^R$ to derive spectral methods.

3.2. **Expansion of the distribution function f.** Hereafter, we use just one index to denote the d-dimensional sums with respect to the vector $k = (k_1, .., k_d) \in \mathbb{Z}^d$, hence we set $|k| := \max\{|k_i|, 1 \leq i \leq d\}$ and the approximate function f_N is represented as the truncated Fourier series with $N = (n, \ldots, n)$ and

$$f_N(v) = \sum_{|k| \leq n} \hat{f}_k \, e^{i \frac{\pi}{L} k \cdot v}, \tag{3.4}$$

with the Fourier coefficient $\hat{f}_k$ given by

$$\hat{f}_k = \frac{1}{(2L)^d} \int_{\mathcal{D}_L} f(v)\, e^{-i \frac{\pi}{L} k \cdot v}\, dv.$$

In a Fourier-Galerkin method the fundamental unknowns are the coefficients $\hat{f}_k(t)$, for $|k| \leq n$. We obtain a set of ODEs for the coefficients $\hat{f}_k$ by requiring that the residual of (3.2) be orthogonal to all trigonometric polynomials of degree less than n. Hence for $|k| \leq n$

$$\int_{\mathcal{D}_L} \left(\frac{\partial f_N}{\partial t} - \mathcal{Q}^R(f_N) \right) e^{-i \frac{\pi}{L} k \cdot v}\, dv = 0.$$

By substituting expression (3.4) in (3.3) we get

$$\mathcal{Q}^R(f_N) \;\; = \;\; \sum_{|l| \leq n} \sum_{|m| \leq n} \hat{\beta}(l, m)\, \hat{f}_l \, \hat{f}_m \, e^{i \frac{\pi}{L} (l+m) \cdot v}, \tag{3.5}$$

where the *kernel modes* $\hat\beta$ are defined by

$$\hat\beta(l,m) = \int_{\mathcal{C}_R} \mathcal{B}(y,z)\,\left[e^{i\frac{\pi}{L}\left(l\cdot\Theta'(y)+m\cdot\Theta'_\star(y)\right)} - e^{i\frac{\pi}{L}m\cdot\Theta_\star(y)}\right] dy. \tag{3.6}$$

3.3. **Projection of the quadratic operator $\mathcal{Q}^R(f_N)$.** The *spectral equation* is the projection of the collision equation in $\mathbb{P}_N$, the $(2n+1)^d$-dimensional vector space of trigonometric polynomials of degree at most n in each direction, with $N=(n,\dots,n)$ *i.e.*,

$$\frac{\partial f_N}{\partial t} = \mathcal{P}_N\,\mathcal{Q}^R(f_N),$$

where $\mathcal{P}_N$ denotes the orthogonal projection on $\mathbb{P}_N$ in $L^2(\mathcal{D}_L)$. A straightforward computation leads to the following set of ordinary differential equations on the Fourier coefficients

$$\frac{\partial \hat f_k}{\partial t} = \sum_{\substack{l+m=k\\ |l|,|m|\le n}} \hat\beta(l,m)\,\hat f_l\,\hat f_m, \quad |k|\le n.$$

3.4. **Application I: the classical spectral method.** In the classical spectral method [31], a simple change of variables in (2.2) permits to write

$$\mathcal{Q}(f) = \int_{\mathbb{R}^d}\int_{\mathbb{S}^{d-1}} \mathcal{B}^{\rm c}(u,\sigma)\big(f(v')f(v'_\star) - f(v)f(v_\star)\big)\,d\sigma\,du, \tag{3.7}$$

with $u=v-v_\star\in\mathbb{R}^d$, $\sigma\in\mathbb{S}^{d-1}$, and

$$\left\{\begin{array}{l} v' = v - \frac{1}{2}(u-|u|\sigma),\\ v'_\star = v - \frac{1}{2}(u+|u|\sigma),\\ v_\star = v + u. \end{array}\right. \tag{3.8}$$

Then, we set $\mathcal{C}:=\mathbb{R}^d\times\mathbb{S}^{d-1}$ and

$$\Theta'(u,\sigma) := -\frac{1}{2}(u-|u|\sigma), \quad \Theta'_\star(u,\sigma) := -\frac{1}{2}(u+|u|\sigma), \quad \Theta_\star(u,\sigma) := u.$$

Finally the collision kernel $\mathcal{B}^{\rm c}$ is defined by

$$\mathcal{B}^{\rm c}(u,\sigma) = B\big(|u|,\hat u\cdot\sigma\big), \quad \text{with} \quad \hat u = \frac{u}{|u|}. \tag{3.9}$$

Thus, the Boltzmann operator (3.7) is now written in the form (3.1). Therefore, we consider a distribution function f such that supp $(f)\subset\mathcal{B}_S$, where $\mathcal{B}_s$ is the ball centred in 0 with radius $S>0$, the domain of the Boltzmann integral operator is then reduced to $\mathcal{B}_R\times\mathbb{S}^{d-1}$ with $R\ge 2S$ and the computational domain $\mathcal{D}_L=[-L,L]^d$ is chosen in order to prevent intersections of the regions where f is different from zero when we compute discrete convolution based on FFT (this is the so-called *dealiasing condition*), that is, $L\ge(3+\sqrt{2})S/2$ (we refer to [31] for a precise explanation of this choice). The truncated operator reads in this case

$$\mathcal{Q}^R(f)(v) = \int_{\mathcal{B}_R\times\mathbb{S}^{d-1}} \mathcal{B}^{\rm c}(u,\sigma)\,\big(f(v'_*)f(v') - f(v_*)f(v)\big)\,d\sigma\,du.$$

Then, we apply the spectral algorithm (3.5) and get for the *kernel modes* (3.6),

$$\hat\beta^c(l,m) = \int_{\mathcal{B}_R}\int_{\mathbb{S}^{d-1}} B(|u|,\cos\theta)\,\left[e^{-i\frac{\pi}{L}\left(u\cdot\frac{(l+m)}{2}-i|u|\sigma\cdot\frac{(m-l)}{2}\right)} - e^{-i\frac{\pi}{L}u\cdot m}\right] d\sigma\,du.$$

Using the conservation of momentum $\Theta' + \Theta'_\star = \Theta_\star$, we recover the algebraic structure of the Boltzmann operator where the loss term is an exact convolution,

$$\hat{\beta}^c(l,m) = \beta^c(l,m) - \beta^c(m,m),$$

with

$$\beta^c(l,m) = \int_{\mathcal{B}_R}\int_{\mathbb{S}^{d-1}} B(|u|,\cos\theta)\, e^{-i\frac{\pi}{L}\left(u\cdot\frac{(l+m)}{2} - i|u|\sigma\cdot\frac{(m-l)}{2}\right)}\, d\sigma\, du.$$

Let us emphasize that explicit computations of Fourier coefficients $\beta^c(l,m)$ have been done in [31, 19] in the VHS case where B is given by (2.3) :

$$\beta(l,m) = 16\, C_\gamma\, \pi^2 (2\lambda\pi)^{3+\gamma} F_\gamma(\xi,\eta),$$

where

$$F_\gamma(\xi,\eta) \equiv \int_0^1 r^{2+\gamma}\, \mathrm{Sinc}(\xi r)\, \mathrm{Sinc}(\eta r)\, dr$$

where $\xi = |l+m|\lambda\pi$, $\eta = |l-m|\lambda\pi$ and $r = |g|/2\lambda\pi$ with $\lambda = 2/(3+\sqrt{2})$. For integer values of γ, F_γ has an explicit analytical expression.

3.5. **Application II: the fast spectral method.** Here we shall approximate the collision operator starting from a representation which conserves more symmetries of the collision operator when one truncates it in a bounded domain. This representation was used in [4, 24] to derive finite differences schemes and it is close to the classical Carleman representation (cf. [7]). Hence, the collision operator (2.2) can be written as

$$\mathcal{Q}(f)(v) = \int_{\mathbb{R}^d\times\mathbb{R}^d} \mathcal{B}^{\mathrm{f}}(y,z)\, \delta(y\cdot z)\big[f(v+z)f(v+y) - f(v+y+z)f(v)\big]\, dy\, dz, \tag{3.10}$$

with

$$\mathcal{B}^{\mathrm{f}}(y,z) = 2^{d-1}\, B\left(|y+z|, -\frac{y\cdot(y+z)}{|y|\,|y+z|}\right)\, |y+z|^{-(d-2)}.$$

Thus, the collision operator is now written in the form (3.1) with $\mathcal{C} := \mathbb{R}^d \times \mathbb{R}^d$,

$$\mathcal{B}(y,z) = \mathcal{B}^{\mathrm{f}}(y,z)\, \delta(y\cdot z),$$

and

$$v'_\star = v + \Theta'_\star(y,z), \quad v' = v + \Theta'(y,z), \quad v_\star = v + \Theta_\star(y,z),$$

with

$$\Theta'_\star(y,z) := z, \quad \Theta'(y,z) := y, \quad \Theta_\star(y,z) := y+z.$$

To compute the computational domain, we proceed as before if f has compact support included in $\mathcal{B}_S$, we have $R = 2S$ and choose $L \geq (3\sqrt{2}+1)S/2$. Then the domain of the Boltzmann integral operator is reduced to $\mathcal{B}_R \times \mathbb{S}^{d-1}$ and the computational domain $\mathcal{D}_L = [-L,L]^d$. The (truncated) operator now reads

$$\mathcal{Q}^R(f)(v) = \int_{\mathcal{C}_R} \mathcal{B}^{\mathrm{f}}(y,z)\, \delta(y\cdot z)\, \big(f(v+z)f(v+y) - f(v+y+z)f(v)\big)\, dy\, dz, \tag{3.11}$$

for $v \in \mathcal{D}_L$. This representation of the collision kernel yields better decoupling properties between the arguments of the operator and allows to lower significantly the computation cost of the method by using the fast Fourier transform (see [26, 18]). From now, we can apply the spectral algorithm (3.5) to this collision operator and the corresponding kernel modes (3.6) are given by

$$\hat{\beta}^f(l,m) = \int_{B_R}\int_{B_R} \mathcal{B}^{\mathrm{f}}(y,z)\, \delta(y\cdot z)\, \left[e^{i\frac{\pi}{L}\left(l\cdot y + m\cdot z\right)} - e^{i\frac{\pi}{L}\, m\cdot\left(y+z\right)}\right]\, dy\, dz.$$

As before, the kernel $\hat{\beta}^f(l,m)$ can be written as

$$\hat{\beta}^f(l,m) = \beta^f(l,m) - \beta^f(m,m),$$

with

$$\beta^f(l,m) = \int_{B_R}\int_{B_R} \mathcal{B}^{\mathrm{f}}(y,z)\,\delta(y\cdot z)\,e^{i\frac{\pi}{L}\left(l\cdot y + m\cdot z\right)}\,dy\,dz.$$

Now we consider the case of Maxwellian molecules in dimension $d=2$, and hard spheres in dimension $d=3$ (the most relevant kernel for applications) for which $\mathcal{B}^f$ is constant $\mathcal{B}^f = \mathcal{C}$.

We first change to spherical coordinates and then we integrate first e' on the intersection of the unit sphere with the plane $e^\perp$, then we get

$$\beta^f(l,m) = \frac{\mathcal{C}}{4}\int_{\mathbb{S}^{d-1}} \phi_R(l\cdot e)\,\left[\int_{\mathbb{S}^{d-1}} \delta(e\cdot e')\,\phi_R(m\cdot e')\,de'\right]\,de,$$

where using the parity of the sin function, we only have

$$\phi_R(s) = \int_{-R}^{R} |\rho|^{d-2}\cos\left(\frac{\pi}{L}\rho s\right)\,d\rho.$$

Moreover, thanks to the parity property of ϕ_R we can adopt the following parametrization

$$\beta^f(l,m) = \mathcal{C}\int_{\mathbb{S}^{d-1}_+} \phi_R(l\cdot e)\,\left[\int_{\mathbb{S}^{d-1}_+} \delta(e\cdot e')\,\phi_R\big(m\cdot e'\big)\,de'\right]\,de,$$

where $\mathbb{S}^{d-1}_+$ denotes the half-sphere. Now since the function $e\mapsto\phi_R(l\cdot e)$ is periodic on $\mathbb{S}^{d-1}_+$; we take a spherical parametrization of $\mathbb{S}^{d-1}_+$ and a uniform grid of size M for the angle discretization, it yields

$$\beta^f(l,m) \;\simeq\; \mathcal{C}\,\frac{\mathrm{m}(\mathbb{S}^{d-1}_+)}{M}\sum_{p=1}^{M}\alpha_p(m)\,\alpha'_p(l), \tag{3.12}$$

where $\mathrm{m}(\mathbb{S}^{d-1}_+)$ represents the size of the domain parametrizing the unit sphere and α_p, α'_p are defined according to a quadrature formula. Therefore, this latter approximation allows to construct a fast algorithm for the gain term as a sum of discrete convolutions.

Let us emphasize that the decomposition (3.12) is possible for various kernels up to a quadrature formula based for instance to a multipole expansion but in that case the expression of β^f is complicated. Here we give two examples, which lead to a nice expression of the kernel $\beta^f(l,m)$: the first one is in $2d_v$ for Maxwellian molecules, that is, $B\equiv 1$ and the second one is in $3d_v$ for hard sphere molecules $B(u,\cos(\theta)) = C\,|u|$.

Example 3.1. *For $d=2$ and Maxwellian molecules, that is, $B(u,\cos(\theta))=1$, then $\mathcal{B}^f(y,z)=2$ and*

$$\phi_R(s) = 2\,R\,\mathrm{Sinc}\left(\frac{\pi R\,s}{L}\right).$$

The kernel $\beta^f(l,m)$ can be decomposed as

$$\beta^f(l,m) \;=\; 2\;\times\;\frac{\pi}{M}\sum_{p=0}^{M-1}\alpha_p(l)\alpha'_p(m)$$

with

$$\alpha_p(l) = \phi_R(l\cdot e_p),\quad \alpha'_p(m) = \phi_R(m\cdot e'_p),$$

where $e_p = (\cos\theta_p,\sin\theta_p)$, $e'_p = (-\sin\theta_p,\cos\theta_p)$ and M is the number of equally spaced points in $[0,\pi]$ and $\theta_p = \pi\,p/M$.

Example 3.2. *For $d = 3$ and hard sphere molecules, that is, $B(u, \cos(\theta)) = |u|$. Thus, $\mathcal{B}^f(x, y) = 4$ and the function ϕ_R is given by*

$$\phi_R(s) = R^2 \left[2\mathrm{Sinc}\left(\frac{\pi R\, s}{L}\right) - \mathrm{Sinc}^2\left(\frac{\pi R\, s}{2L}\right)\right].$$

The kernel $\beta^f(l, m)$ can be decomposed as

$$\beta^f(l, m) \;=\; \frac{4\pi^2}{M^2} \sum_{p=1}^{M} \sum_{q=1}^{M} \alpha_{p,q}(l)\, \alpha'_{p,q}(m)$$

with

$$\begin{cases} \alpha_{p,q}(l) = \phi_R(l \cdot e_{p,q}) \sin(\varphi_q), \\ \\ \alpha'_p(m) = \displaystyle\int_{\mathbb{S}^2_+ \cap e^{\perp}_{p,q}} \phi_R(m \cdot e')de' \;=\; \int_0^{\pi} \phi_R\left(|\Pi_{e^{\perp}_{p,q}}(m)| \cos\theta\right) d\theta, \end{cases}$$

where M^2 is the number of equally spaced points in $[0, \pi]^2$ and the unit vector $e_{p,q}$ is given by $e_{p,q}$ $= (\cos\theta_p \sin\varphi_q,\ \sin\theta_p \sin\varphi_q,\ \cos\varphi_q)$, for $\theta_p = p\pi/M$ and $\varphi_q = q\pi/M$, $p, q \in \{1, M\}$.

4. Space and time discretization

In this section, we first focus on the discretization of the transport step and omit for sake of clarity the collisional operator and the velocity variable is fixed $v_l = l\Delta v \in \mathbb{R}^d$, with $l = (l_1, \cdots, l_d) \in \mathbb{Z}^d$

$$\begin{cases} \dfrac{\partial f}{\partial t} \;+\; v \cdot \nabla_x f \;=\; 0,\ \forall\, (t, x) \;\in \mathbb{R}^+ \times \Omega, \\ \\ f(t = 0, x, v) = f_0(x, v),\ \ x \in \Omega,\ \ v \in \mathbb{R}^d. \end{cases} \tag{4.13}$$

We shall develop the scheme in the context of Finite Volume methods for the approximation of the transport part. We consider $\mathcal{T}$ a mesh of the space domain $\Omega \subset \mathbb{R}^d$. For any control volume $T_i \in \mathcal{T}$ we denote by $\mathcal{N}(i)$ the set of the neighbours of i. If $j \in \mathcal{N}(i)$, $\sigma_{i,j}$ is the common interface between T_i and T_j and $n_{\sigma_{i,j}}$ is the unit normal vector to $\sigma_{i,j}$ oriented from T_i to T_j and we have $n_{\sigma_{i,j}} = -n_{\sigma_{j,i}}$. Let m_i be the Lebesgue measure of the control volume T_i, $\Delta t > 0$ be the time step and $t^n = n\,\Delta t$. We set $f_i^n(v_l)$ an approximation of the distribution function at time t^n in the control volume T_i

$$f_i^n(v_l) \simeq \frac{1}{m_i} \int_{T_i} f(t^n, x, v_l)dx.$$

We integrate the transport equation (4.13) over the control volume $[t^n, t^{n+1}] \times T_i$ and then construct a discrete approximation which satisfies

$$\begin{cases} m_i \dfrac{f_i^{n+1}(v_l) - f_i^n(v_l)}{\Delta t} + \displaystyle\sum_{j \in \mathcal{N}(i)} \mathcal{F}^n(v_l, \sigma_{i,j}) = 0, \quad T_i \in \mathcal{T},\ n \in \mathbb{N}, \\ \\ f_i^0(v_l) = \dfrac{1}{m_i} \displaystyle\int_{T_i} f_0(x, v)dx, \end{cases} \tag{4.14}$$

where $\mathcal{F}^n(v_l, \sigma_{i,j})$ represents a numerical flux on $[t^n, t^{n+1}] \times \sigma_{i,j}$

$$\mathcal{F}^n(v_l, \sigma_{i,j}) = m(\sigma_{i,j})\ \left(v \cdot n_{\sigma_{i,j}}\right)\ f_{i,j}^n(v_l)$$

and $f^n_{i,j}$ is an approximation of the edge-based fluxes between times t^n and t^{n+1}. This formula defines a class of finite volume schemes. For instance a second order upwind scheme is obtained by taking

$$f^n_{i,j}(v_l) = \begin{cases} f^n_i(v_l) \,+\, \delta_{i,j} \,\left(f^n_j(v_l) - f^n_i(v_l) \right), \text{ if } \left(v \cdot n_{\sigma_{i,j}} \right) \,>\, 0, \\ \\ f^n_j(v_l) \,+\, (1-\delta_{i,j}) \,\left(f^n_i(v_l) - f^n_j(v_l) \right), \text{ else,} \end{cases}$$

where $\delta_{i,j}$ defines a slope limiter such that for all $k \in \mathcal{N}(i)$ there exists $0 < \beta_{i,k} < 1$ satisfying

$$\begin{cases} 0 \le \displaystyle\sum_{\substack{k\in\mathcal{N}(i),\\ k\neq j}} \beta_{i,k} \le 1, \\ \\ \delta_{i,j} \,\left(f^n_j(v_l) - f^n_i(v_l) \right) = \displaystyle\sum_{\substack{k\in\mathcal{N}(i),\\ k\neq j}} \beta_{i,k} \left(f^n_i(v_l) - f^n_k(v_l) \right). \end{cases}$$

4.1. **Boundary conditions.** The most difficult part in the actual implementation of finite volume methods for kinetic equations is that of boundary conditions. We will discuss here the situation of solid walls.

Let σ_i be an edge of the control volume T_i, with $\sigma_i \in \partial\Omega$ and let us denote by $n(\sigma_i)$ a unit outer vector to the edge σ_i. We define the boundary solution on σ_i by

$$f^n_{\sigma_i}(v_l) = \begin{cases} (1-\alpha)\, \mathcal{R}\, f^n_{\sigma_i}(v_l) \;+\; \alpha\, \mathcal{M}\, f^n_{\sigma_i}(v_l), \text{ if } v \cdot n(\sigma_i) \ge 0, \\ \\ f^n_i(v_l), \text{ if } v \cdot n(\sigma_i) < 0, \end{cases} \tag{4.15}$$

where $\mathcal{R} f^n_{\sigma_i}(v_l)$ and $\mathcal{M} f^n_{\sigma_i}(v_l)$ are defined by (2.6). On the one hand, we compute an approximation of the operator describing specular reflection $\mathcal{R} f^n_{\sigma_i}(v_l)$, it gives for $v_l \cdot n(\sigma_i) \ge 0$,

$$\mathcal{R}^* f^n_{\sigma_i}(v_l) = f^n_{\sigma_i}(v^*), \quad \text{with } v^* \,=\, v_l - 2(v_l \cdot n(\sigma_i))\, n(\sigma_i).$$

Unfortunately, the distribution function $f^n_{\sigma_i}(.)$ is not necessarily known on v^* and a piecewise linear interpolation is applied to compute the value at v^*. Then, to guarantee the local flux conservation we modify the boundary solution by considering the re-normalized boundary solution for $v_l \cdot n(\sigma_i) \ge 0$

$$\mathcal{R} f^n_{\sigma_i}(v_l) \,=\, \xi^n(\sigma_i)\; \mathcal{R}^* f^n_{\sigma_i}(v_l), \tag{4.16}$$

where the nonnegative constant $\xi^n(\sigma_i)$ is given by

$$\xi^n(\sigma_i)\, \Delta v^d \sum_{v_l \cdot n(\sigma_i) \ge 0} v_l \cdot n(\sigma_i)\, f^n_{\sigma_i}(v_l) \;=\; -\Delta v^d \sum_{v_l \cdot n(\sigma_i) < 0} v_l \cdot n(\sigma_i)\, f^n_i(v_l).$$

Clearly $\mathcal{R}\, f^n_{\sigma_i}$ is constructed to guarantee a global zero flux property at the boundary σ_i and preserves nonnegativity of the distribution at the boundary.

On the other hand, diffusive boundary conditions are also implemented such that the global flux at the boundary

$$\mathcal{M} f^n_{\sigma_i}(v_l) \,=\, \mu^n(\sigma_i)\, \exp\left(-\frac{v_l^2}{2 k_B T_w} \right), \tag{4.17}$$

where the constant $\mu^n(\sigma_i) \geq 0$ is computed to ensure the zero flux condition on $\sigma_i \subset \partial\Omega$

$$\mu^n(\sigma_i)\,\Delta v^d \sum_{v_l\cdot n(\sigma_i)\geq 0} v_l\cdot n(\sigma_i)\,\exp\left(-\frac{v_l^2}{2k_BT_w}\right) \;=\; -\Delta v^d \sum_{v_l\cdot n(\sigma_i)<0} v_l\cdot n(\sigma_i)\,f_i^n(v_l).$$

From this construction, we easily prove the following property, which is the analogous result of Proposition 2.1.

Proposition 4.1. *The scheme (4.14) supplemented with the discrete boundary conditions (4.15)-(4.17) satisfies for all $n \in \mathbb{N}$ and $\sigma_i \in \partial\Omega$*

$$\sum_l \Delta v^d\,\mathcal{F}^n(v_l,\sigma_i) = 0.$$

Moreover, global mass is preserved over time

$$\sum_l \Delta v^d m_i f_i^n(v_l) \;=\; \sum_l \Delta v^d m_i f_i^0(v_l).$$

4.2. **Stable time discretization.** Another difficulty in the numerical resolution of the Boltzmann equation (2.1) is due to the nonlinear stiff collision (source) terms induced by small mean free or relaxation time. In [20], we propose to penalize the nonlinear collision term by a BGK-type relaxation term, which can be solved explicitly even if discretized implicitly in time. Since the convection term in (2.1) is not stiff, we will treat it explicitly. The source terms on the right hand side of (2.1) will be handled using the ODE solver in the previous section. For example, if a first order IMEX scheme is used, we have [20]

$$\left\{\begin{array}{l} m_i\dfrac{f_i^{n+1}-f_i^n}{\Delta t} + \displaystyle\sum_{j\in\mathcal{N}(i)} \mathcal{F}^n(v_l,\sigma_{i,j}) \;=\; m_i\dfrac{\mathcal{Q}(f_i^n)\;-\;\mathcal{P}(f_i^n)}{\varepsilon} \;+\; m_i\,\dfrac{\mathcal{P}(f_i^{n+1})}{\varepsilon}, \\[2ex] f_i^0(v_l) = \dfrac{1}{m_i}\displaystyle\int_{T_i} f_0(x,v_l)dx\,. \end{array}\right. \tag{4.18}$$

Using the relaxation structure of $\mathcal{P}(f)$ given by

$$\mathcal{P}(f) \;=\; \lambda\,(\,\mathcal{M}[\rho,u,T](v)\;-\;f(v)\,),$$

where $\lambda := C_0\,2\pi\,\rho$ for Maxwellian molecule in $2d_v$ and λ is chosen $\lambda \geq L(f)$ in the general case, (4.18) can be written as

$$\begin{aligned} m_i\,f_i^{n+1} \;&=\; \frac{\varepsilon}{\varepsilon+\lambda^{n+1}\Delta t}\left(m_i\,f_i^n - \Delta t\sum_{j\in\mathcal{N}(i)}\mathcal{F}^n(v,\sigma_{i,j})\right) \;+\; \Delta t\,m_i\,\frac{\mathcal{Q}(f_i^n)\;-\;\mathcal{P}(f_i^n)}{\varepsilon+\lambda^{n+1}\Delta t} \\ &\quad +\; m_i\,\frac{\lambda^{n+1}\Delta t}{\varepsilon+\lambda^{n+1}\Delta t}\,\mathcal{M}_i^{n+1}, \end{aligned} \tag{4.19}$$

where $\lambda^n = \lambda[\rho^n,T^n]$ and $\mathcal{M}_i^n$ is the local Maxwellian distribution $\mathcal{M}[\rho^n,u^n,T^n]$ computed from f_i^n in the control volume T_i. Moreover, a second order IMEX scheme can also be implemented [20].

Let us mention that a similar approach is proposed by G. Dimarco & L. Pareschi using exponential Runge-Kutta methods for stiff kinetic equations [12].

5. Numerical tests

In this section, we present a large variety of test cases in $1d_x \times 2d_v$ and $2d_x \times 2d_v$ showing the effectiveness of our method to get an accurate solution of the Boltzmann equation. Since we only consider two dimensional velocity problems we restrict ourselve to Maxwellian molecules kernel in order to apply the fast algorithm. However, let us emphasize that our approach also includes the more realistic case $3d_v$ problems with hard sphere but the computational cost is in that case much more important. We first give some examples (propagation of discontinuities, flow generated by gradients of temperature and Poiseuille flow), which have already been treated by DSMC.

Finally, we present two numerical results in $1d_x \times 2d_v$ for the trend to equilibrium of the solution to the nonlinear Boltzmann equation with specular reflection at the boundary and in the $2d_x \times 2d_v$ dimensional phase space, we reproduce small effects (ghost effects) in the asymptotic limit ε goes to zero by considering diffusive boundary conditions. The solution is then compared with the one obtained by discretizing the Navier-Stokes equations in order to illustrate the non validity of the Navier-Stokes equations in this limit.

5.1. **Propagation of discontinuities.** This first test is devoted to the numerical approximation of the distribution function by the fast spectral method for discontinuous solutions. Of course in that case, spectral accuracy cannot be achieved and any numerical method cannot be more than first order accurate. We consider the Boltzmann equation

$$\left\{ \begin{array}{l} \dfrac{\partial f}{\partial t} + v_x \dfrac{\partial f}{\partial x} = \dfrac{1}{\varepsilon} \mathcal{Q}(f), \\ \\ f(t=0) = f_0, \end{array} \right.$$

with $\varepsilon = 0.1$, an initial datum f_0 which is a constant state in space and a Maxwellian distribution function in velocity with a temperature T_0,

$$f_0(x,v) = \frac{1}{(2\pi k_B T_0)} \exp\left(-\frac{|v|^2}{2k_B T_0} \right), \quad x \in (-0.5,\, 0.5),\, v \in \mathbb{R}^2,$$

with $k_B = T_0 = 1$. Then, at time $t = 0$, we suddenly change the temperature at the boundary $x = -1/2$, where we consider purely diffusive boundary conditions with a wall temperature $T_w = 2\,T_0$. Therefore, a discontinuous distribution function in velocity is generated at the boundary and propagates in the physical domain, then it is damped due to the effect of the collision operator.

Notice that I. Gamba & S. H. Tharkabhushanam [21, 22] already performed such numerical simulations in $1d_x \times 3d_v$ using the method based on the Fourier transform [4]. Here, we want to illustrate the effect of the angle discretization (3.12) for discontinuous solutions. Indeed, in [26] it has been shown that for smooth solutions, the angle discretization parameter M does not affect the accuracy of the spectral method and can be chosen small, that is $M \simeq 4$.

We present several numerical simulations with $\Delta t = 0.001$, the final time is $t_{end} = 1$, a computational domain in space $x \in [-1/2, 1/2]$ with $n_x = 128$, a domain in velocity $[-8, 8]^2$, and take respectively $n = 32$, 64 and 128 and also choose several values for $M = 4$, 8 and 12. Surprisingly, we still observe a good agreement between the different numerical results even when M is small. Actually, we cannot distinguish the curves for the different values of $n = 32$, 64 and 128, but also of $M = 4$, 8 and 12 (see Figure 1).

In Figure 1-(4), we present the time evolution of the distribution function at $x = -0.4961$ on the right hand side of the wall for $n = 32$ with $M = 4$, 8 and $n = 128$ with $M = 16$. Let us notice that for $n = 32$, which is relatively small, the discontinuity of the distribution function is a bit smeared but we do not observe any spurious osccilations. The smearing is only due to the fact that there are few points to describe the discontinuous function.

Also, let us emphasize that the spectral algorithm applied to discretize the Boltzmann collision operator does not preserve the nonnegativity of the distribution function. However, the algorithm does not produce spurious oscillations even if for large velocities, some negative values may be induced, they do not affect the accuracy of the results.

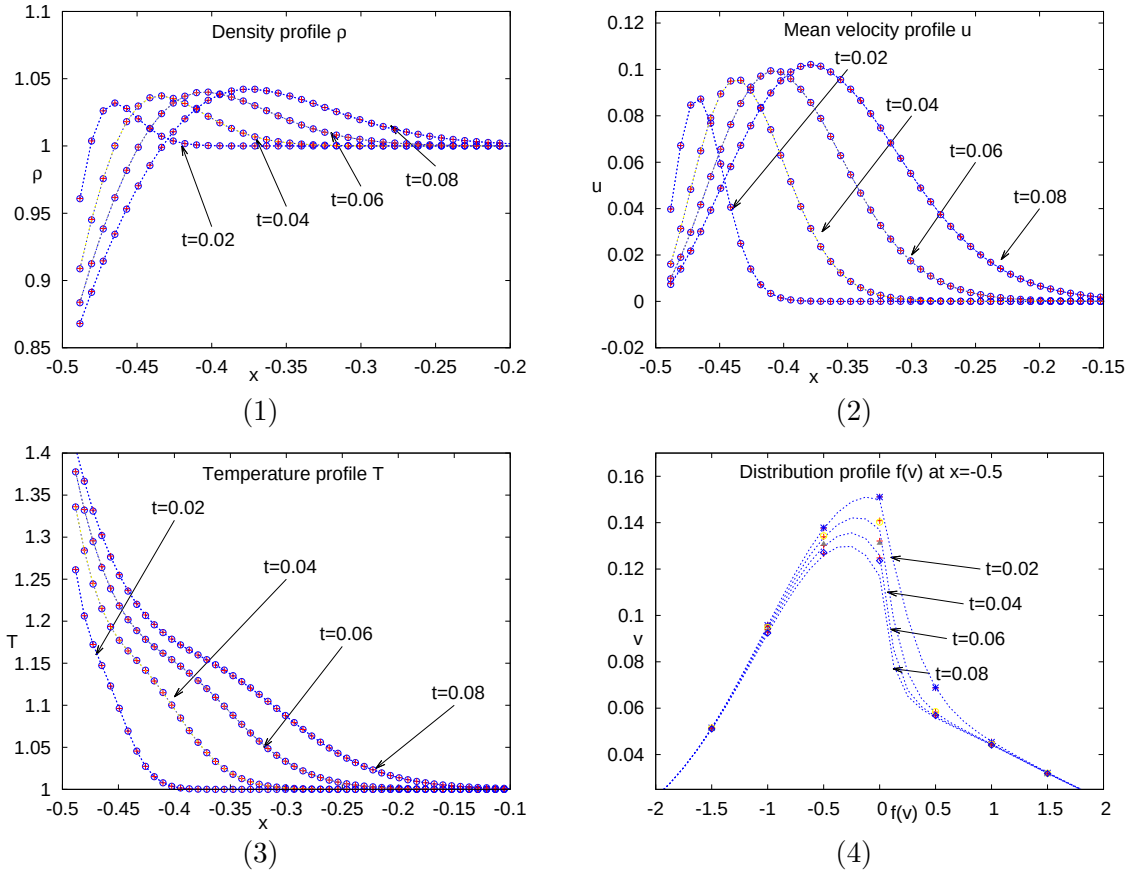

FIGURE 1. Propagation of discontinuities: *(1) density (2) mean velocity (3) temperature and (4) zoom of the distribution function at* $x = -0.4961$ *for* $n = 32$ *and various numbers of angle discretization* $M = 4$, 8 *with dots and* $n = 128$, $M = 16$ *with lines.*

Finally the results are in good agreement with those presented in [21, 22] and surprisingly the accuracy does not become worse when the number of angle discretization M becomes small. Therefore, the fast algorithm seems to be very robust and accurate even for non smooth distribution functions.

5.2. **Flow generated by a gradient of temperature.** We consider the Boltzmann equation (2.1)-(2.2),

$$\begin{cases} \dfrac{\partial f}{\partial t} + v_x \dfrac{\partial f}{\partial x} \;=\; \dfrac{1}{\varepsilon}\, \mathcal{Q}(f), \;\; x \in (-1/2, 1/2), \; v \in \mathbb{R}^2, \\ \\ f(t=0,x,v) = \dfrac{1}{2\pi\, k_B\, T_0(x)} \, \exp\left(-\dfrac{|v|^2}{2 k_B\, T_0(x)} \right), \end{cases}$$

with $k_B = 1$, $T_0(x) = 1 + 0.44\,(x - 1/2)$ and we assume purely diffusive boundary conditions on $x = -1/2$ and $x = 1/2$, which can be written as

$$f(t, x, v) = \mu(t, x)\; f_w(v), \text{ if } (x, v_x) \in \{-1/2\} \times \mathbb{R}^+ \text{ and } (x, v_x) \in \{1/2\} \times \mathbb{R}^-,$$

where μ is given by (2.7). This problem has already been studied in [34] using DSMC for the Boltzmann equation or using deterministic approximation using a BGK model for the Boltzmann equation in [23]. Here we apply our deterministic scheme and choose a computational domain $[-8, 8] \times [-8, 8]$ in the velocity space with a number grid points $n = 32$ in each direction, the number of angle discretization is $M = 4$, whereas for the space direction we take $n_x = 120$ and the time step $\Delta t = 0.001$.

In Figure 2, we represent the stationary solution (obtained approximately at time $t_{end} = 25$ for $\varepsilon = 0.1$ up to $t_{end} = 75$ for $\varepsilon = 0.025$) of the temperature and the pressure profile. The results are in a qualitative good agreement with those already obtained in [34] with DSMC. More precisely, the boundary layer (Knudsen layer) appears in the density and temperature as well as the pressure, but it is small for all the quantities. The magnitude in the dimensionless density, temperature, and pressure is of order of ε and the thickness of the layer is, say $O(3\varepsilon)$. In the density and temperature profiles, we cannot observe it unless we magnify the profile in the vicinity of the boundary (see the zoom in Figure 2). Instead, since the pressure is almost constant in the bulk of the gas, we can observe perfectly the boundary layer by magnifying the entire profile. Let us emphasize that, as it is shown in Figure 2 the Knudsen layer is a kinetic effect, which disappears in the fluid limit ($\varepsilon \to 0$).

These results provide strong evidence that the present deterministic method can be used to determine the state of a gas under highly non-equilibrium conditions. Using deterministic methods, we can investigate the behavior of gases for situations in which molecular diffusion is important e.g., thermal diffusion.

Also let us mention that a quantitative comparison between the present results ($2d_v$ with Maxwell molecule kernel) and [34] ($3d_v$ Boltzmann with hard sphere potential) or [23] ($3d_v$ BGK) shows that the thickness and the amplitude of the Knudsen layer are much more smaller for Maxwell molecules.

5.3. **Poiseuille-type flow driven by a uniform external force.** The Poiseuille flow is a classical example to study by means of the Navier-Stokes equations. Usually the Poiseuille flow is understood to be driven by an externally imposed pressure gradient, but it is trivially equivalent to applying a gravitational force over each particle. For small velocities (small Reynolds or Mach number) the flow is known to be laminar and stationary and the velocity profile is parabolic. There is, however, a critical Knudsen number above which an unstable regime starts and the flow can be described using Burnett equations.

Here, we consider an ideal gas between two parallel infinite plates at rest with a common uniform temperature. When the gas is subject to a uniform external force in the direction parallel to the plates, a steady unidirectional flow of the gas is caused between the plates. Assume that the plates are at rest and located at $x = 0$ and $x = 1$ and kept at temperature $T_w = 1$. The gas is subject to a uniform external force in the y-direction, *i.e.*, in the direction parallel to the plates. There is no pressure gradient in the y-direction. We investigate the steady flow of the gas caused by the external force on the basis of kinetic theory for a wide range of the Knudsen number, paying special attention to the behavior for small Knudsen numbers. Our basic assumptions are as follows:

- the behavior of the gas is described by the Boltzmann model (2.1)-(2.2),
- the gas molecules are reflected diffusely on the plates.

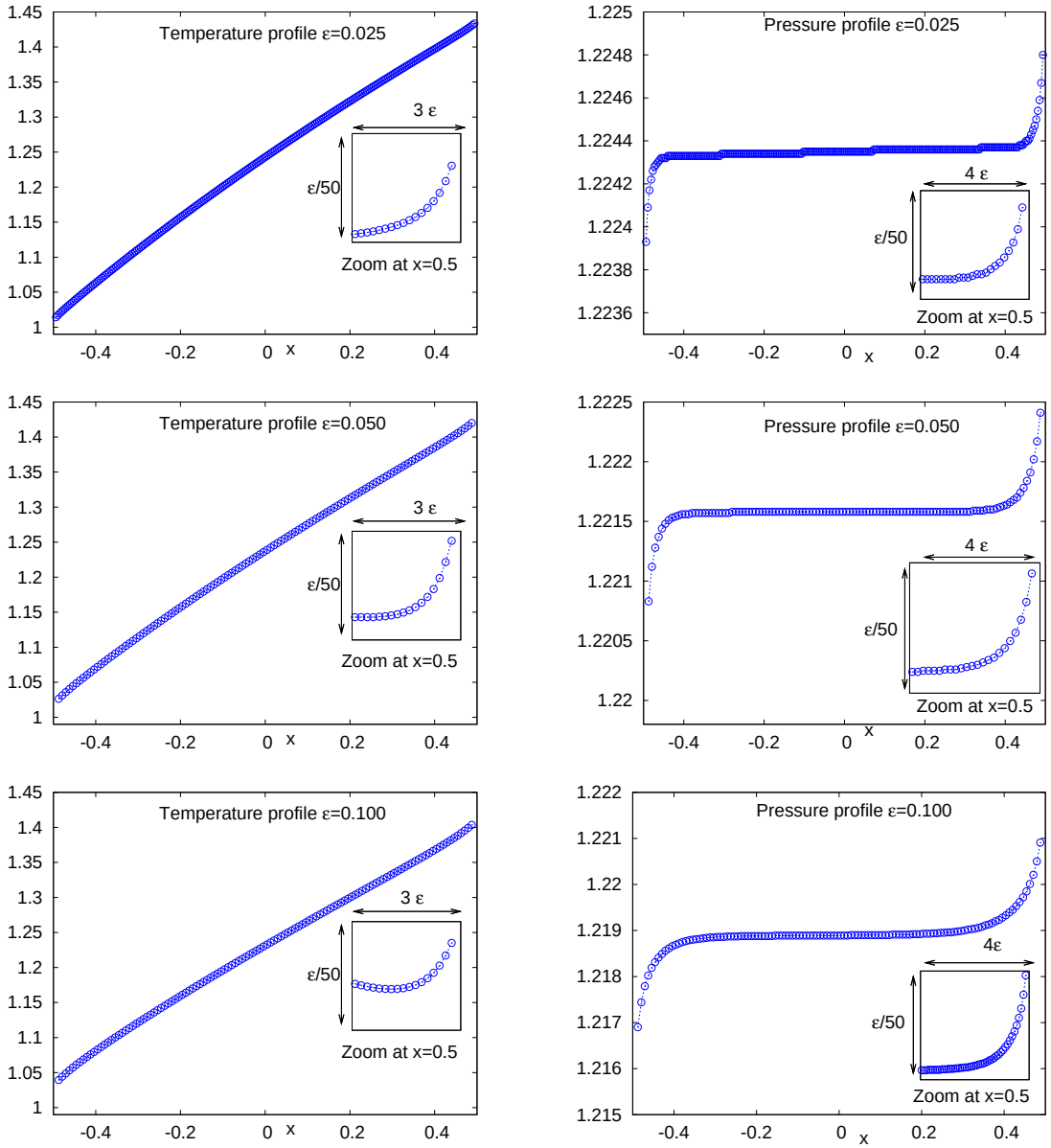

FIGURE 2. Flow generated by a gradient of temperature: *(1) temperature (2) pressure for various Knudsen numbers* $\varepsilon = 0.025,\ 0.05$ *and* 0.1.

The Boltzmann equation in the present problem is written as

$$\begin{cases} \dfrac{\partial f}{\partial t} + v_x \dfrac{\partial f}{\partial x} + a \dfrac{\partial f}{\partial v_y} = \dfrac{1}{\varepsilon} \mathcal{Q}(f), \\ \\ f(t=0) = f_0, \end{cases}$$

with purely diffusive boundary conditions and $a = 0.5$. In this section, we give some numerical results for intermediate values of the Knudsen number in the case where a is fixed. We apply our deterministic scheme and choose a computational domain $[-8,8]\times[-8,8]$ in the velocity space with

a number grid points $n = 32$ in each direction, the number of discrete angles $M = 4$ and for the space direction $n_x = 64$. Finally we take $\Delta t = 0.002$ and the final time is $t_{end} = 35$ for $\varepsilon = 0.3$ and $t_{end} = 100$ for $\varepsilon = 0.05$.

In Figures 3, we show the profiles of the density, flow velocity, and temperature for various Knudsen numbers $\varepsilon > 0$ but for a fixed value of the force parameter $a = 0.5$. In that case, the driven force amplitude a is small and then the flow speed is naturally low, and thus the density and temperature profiles are nonuniform.

We do not present the plot of the pressure, which is not uniform but its non-uniformity is quite small since it is proportional to ϵ^2. The most interesting remark is that the temperature profile is not parabolic and its non-uniformity is dominated by a x^4 term. The temperature at this order has a minimum at the center of the channel but it has symmetric maxima quite near the center as it has been already shown in [38]

The results are in good agreement with those presented in [39] obtained from the BGK model for the Boltzmann equation. It clearly shows that Boltzmann's operator implies a gas-dynamics that has a more complex nature than standard hydrodynamics and most hydrodynamic quantities show boundary effects. Of course, in this simple configuration (a laminar stationary flow), it is still possible to derive analytic perturbative expressions for every hydrodynamic field and compare them with what is obtained in our simulations [38]. The effects beyond standard hydrodynamics is clearly observable, and are correctly described with our numerical scheme.

5.4. **Trend to equilibrium.** We consider the full Boltzmann equation in dimension $d_v = 2$

$$\frac{\partial f}{\partial t} + v \cdot \nabla_x f = \frac{1}{\varepsilon} \mathcal{Q}(f), \quad x \in [0,1], v \in \mathbb{R}^2,$$

with purely specular reflection at the boundary in x. We first introduce the $(d+2)$ scalar fields of density ρ, mean velocity u and temperature T defined by (2.4). Whenever $f(t,x,v)$ is a smooth solution to the Boltzmann equation with specular boundary conditions, one has the global conservation laws for mass and energy. Therefore, without loss of generality we shall impose

$$\int_{[0,1]\times\mathbb{R}^2} f(t,x,v)\, dx\, dv = 1, \quad \int_{[0,1]\times\mathbb{R}^2} f(t,x,v)\, \frac{|v|^2}{2}\, dx\, dv = 1.$$

These conservation laws are then enough to uniquely determine the stationary state of the Boltzmann equation: the normalized global Maxwellian distribution

$$\mathcal{M}_g(v) = \frac{1}{2\pi k_B} \exp\left(-\frac{|v|^2}{2k_B}\right). \tag{5.20}$$

We shall use the following terminology: a velocity distribution of the form (5.20) will be called a *Maxwellian distribution*, whereas a distribution of the form

$$\mathcal{M}_l(t,x,v) = \frac{\rho(t,x)}{2\pi k_B T(t,x)} \exp\left(-\frac{|v-u(t,x)|^2}{2k_B T(t,x)}\right) \tag{5.21}$$

will be called a *local Maxwellian distribution* (in the sense that the constants ρ, u and T appearing there depend on the position x). We also define the notion of *relative local entropy* H_l, the entropy relative to the local Maxwellian, and the *relative global entropy* H_g, the entropy relative to the global Maxwellian distribution, by

$$\mathcal{H}_l(t) = \int f \log\left(\frac{f}{\mathcal{M}_l}\right) dx\, dv, \quad \mathcal{H}_g(t) = \int f \log\left(\frac{f}{\mathcal{M}_g}\right) dx\, dv.$$

Our goal here is to investigate numerically the long-time behavior of the solution f. If f is any reasonable solution of the Boltzmann equation, satisfying certain *a priori* bounds of compactness (in particular, ensuring that no kinetic energy is allowed to leak at large velocities), then it is

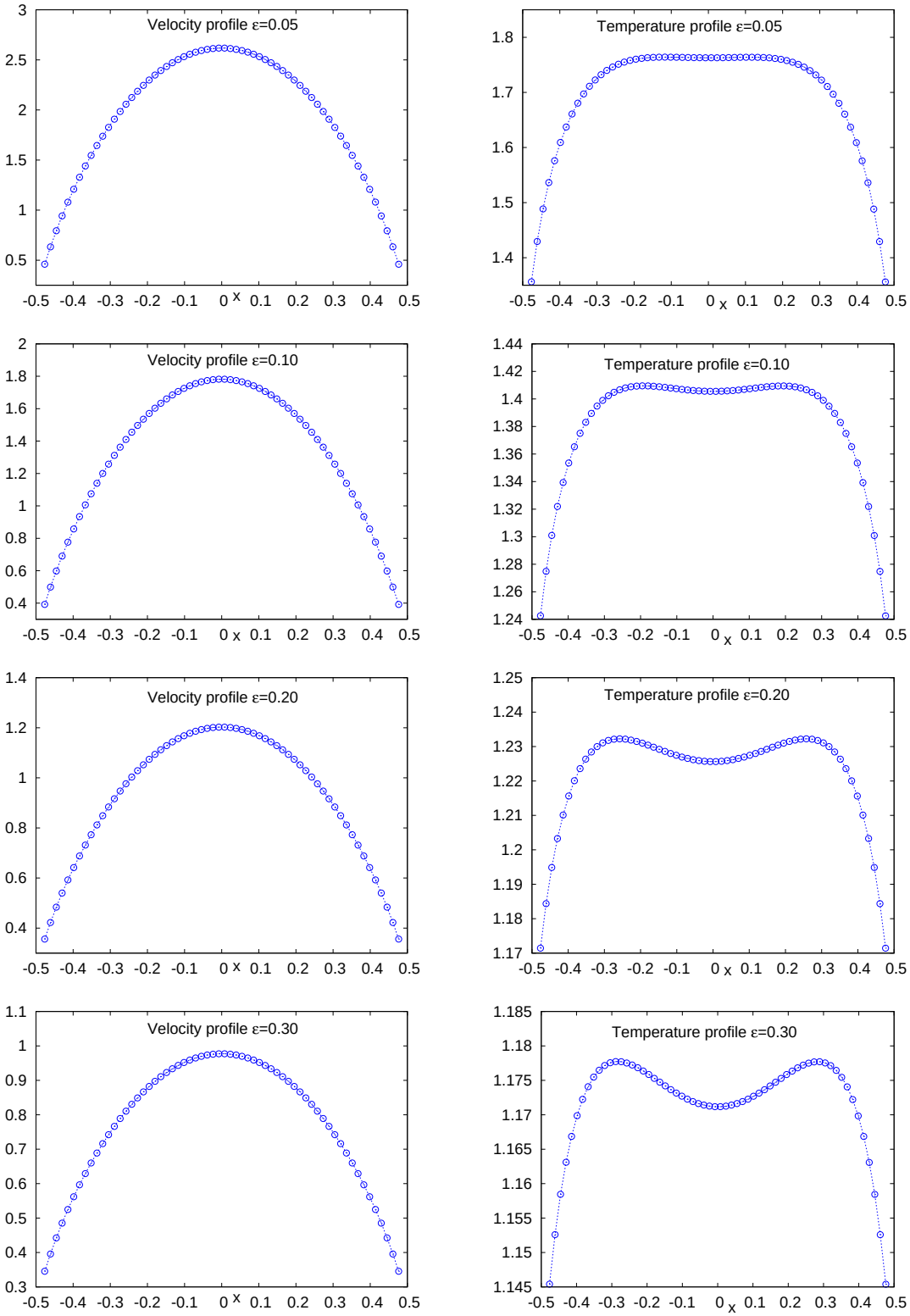

FIGURE 3. Poiseuille flow: *(1) mean velocity and (2) temperature for various Knudsen numbers* $\varepsilon = 0.05,\ 0.1,\ 0.2$ *and* 0.3.

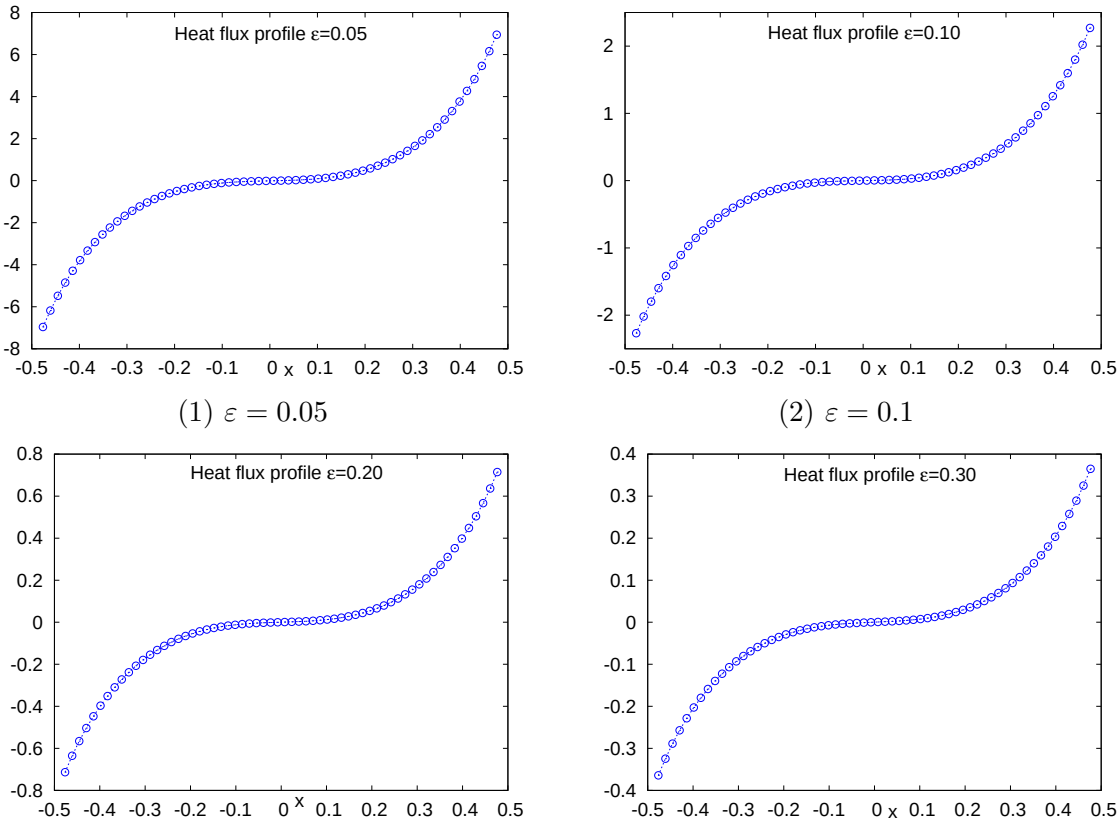

(1) $\varepsilon = 0.05$ (2) $\varepsilon = 0.1$

(3) $\varepsilon = 0.2$ (4) $\varepsilon = 0.5$

FIGURE 4. Poiseuille flow: *heat flux for various Knudsen numbers* $\varepsilon = 0.05$, 0.1, 0.2 *and* 0.3.

possible to prove that f does indeed converge to the global Maxwellian distribution $\mathcal{M}_g$ as t goes to $+\infty$. More recently, Desvillettes and Villani [11], Guo and Strain [37] were interested in the study of rates of convergence for the full Boltzmann equation. Roughly speaking in [11], the authors proved that if the solution to the Boltzmann equation is smooth enough and satisfies bounds from below, then (with constructive bounds)

$$\|f(t) - \mathcal{M}_g\| = O(t^{-\infty}),$$

which means that the solution converges almost exponentially fast to the global equilibrium (namely with polynomial rate $O(t^{-r})$ with r as large as wanted).

The solution f to the Boltzmann equation satisfies the formula of additivity of the entropy: the entropy can be decomposed into the sum of a purely hydrodynamic part, and (by contrast) of a purely kinetic part. In terms of H functional: one can write

$$\mathcal{H}_g(t) = \mathcal{H}_l(t) + \mathcal{H}_h(t),$$

with the hydrodynamic entropy H_h

$$\mathcal{H}_h(t) \;=\; \int_0^1 \rho_l(t,x)\, \log\left(\frac{\rho_l(t,x)}{T_l(t,x)}\right) dx.$$

Moreover in [11], Desvillettes and Villani conjectured that time oscillations should occur on the evolution of the relative local entropy. In fact their proof does not rule out the possibility that the

entropy production undergoes important oscillations in time, and actually most of the technical work is caused by this possibility. In [18], the authors investigate the same problem with periodic boundary conditions and justify the oscillation frequency and damping rate using a spectral analysis of the linearized Boltzmann equation (see [13]).

Here, we performed simulations on the full Boltzmann equation in a simplified geometry (one dimension of space, two dimensions of velocity, with pure specular boundary conditions) for different values of the Knudsen number $\varepsilon > 0$ with the fast spectral method to observe the evolution of the entropy and to check numerically if such oscillations occur. Clearly this test is challenging for a numerical method due to the high accuracy required to capture such oscillating behavior.

Then, we consider an initial datum as a perturbation of the global equilibrium M_g beginequation

$$f_0(x,v) = \frac{1}{2\pi v_{th}^2}\left(1 + A_0\,\sin(2\pi\,x)\right)\,\left[\exp\left(-\frac{|v-v_0|^2}{2T_0(x)}\right) + \exp\left(-\frac{|v+v_0|^2}{2T_0(x)}\right)\right], \tag{5.22}$$

with $v_0 = \frac{1}{\sqrt{5}}\,(1,1)$, the constant $A_0 = 0.2$ and

$$T_0(x) = \frac{2}{\sqrt{5}}\,\left(\,1\,+\,0.1\,\cos(2\pi x)\,\right), \quad x \in [0,1].$$

To get accurate results in the velocity space we take a large domain in velocity $[-9,9]^2$ and $n = 64$, but the number of discrete angles $M = 4$ since this choice does not really affect the accuracy. Also, on the computational domain $x \in [0,1]$, we take $n_x = 100$ and $\Delta t = 0.001$. For this choice, the numerical error is expected to be small since the solution is smooth and the variations of momentum and energy are from 10^{-6} for $\varepsilon = 1$ to 10^{-7} when ε is smaller. Therefore, we stop the numerical simulations when the entropy $\mathcal{H}_l$ approaches this threshold. Moreover, to avoid numerical artefact's due to negative values, we only consider values of f_H, which are above 10^{-10} for the computation of the entropy.

We present the time evolution of the relative entropies $\mathcal{H}_g$, $\mathcal{H}_l$ and $\mathcal{H}_h$ in log scale and observe that initially the entropy is strongly decreasing and when the distribution function becomes close to a local equilibrium, some oscillations appear for small values of $\varepsilon \ll 1$ (see Figure 5). The superimposed curves yield the time evolution respectively of the total $\mathcal{H}_g$ functional, of its kinetic part $\mathcal{H}_l$ and the hydrodynamic entropy $\mathcal{H}_h$.

In Figures 5 and 6, we are indeed able to observe oscillations in the entropy production and in the hydrodynamic entropy, where the strength of the oscillations depends a lot on the parameter ε.

The first plot corresponds to $\varepsilon = 1$ and the second one to $\varepsilon = 0.5$. Some slight oscillations can be seen in the case $\varepsilon = 1$, but what is most striking is that after a short while, the kinetic entropy is very close to the total entropy: an indication that the solution evolves basically in a spatially homogeneous way (contrary to the intuition of the hydrodynamic regime). For $\varepsilon = 0.5$, the kinetic entropy H_l is still non-increasing but after a while it becomes much smaller than the hydrodynamic part and some variations on the decay of the kinetic entropy can be observed.

On the contrary, in the case $\varepsilon = 0.125$ and more clearly for $\varepsilon = 0.05$, the oscillations are much more important but they appear with a small amplitude and the hydrodynamic entropy is relatively closed to the entropy relative to the global equilibrium. Here we are in the hydrodynamic regime and as it has already be mentioned in [18] the oscillation frequency and damping rate of the entropy can be predicted by a precise spectral analysis of the linearized compressible Euler system and compressible Navier-Stokes system.

Further note that the equilibration is much more rapid when ε is small, and that the convergence seems to be exponential. We also observe that the damping rate is related to ε and is in fact proportional to ε when ε becomes small.

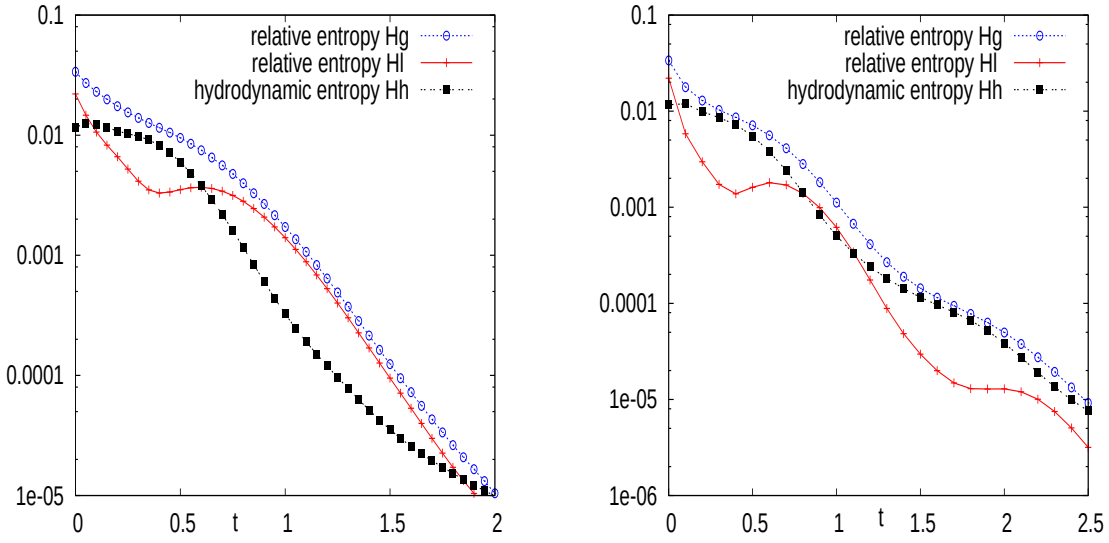

(1) $\varepsilon = 1$ (2) $\varepsilon = 0.5$

FIGURE 5. Trend to equilibrium: *time evolution of the entropy relative to the global equilibrium $\mathcal{H}_g$, entropy relative to the local equilibrium $\mathcal{H}_l$ and hydrodynamic entropy $\mathcal{H}_h$ (1) $\varepsilon = 1$ and (2) $\varepsilon = 0.5$ in log scale.*

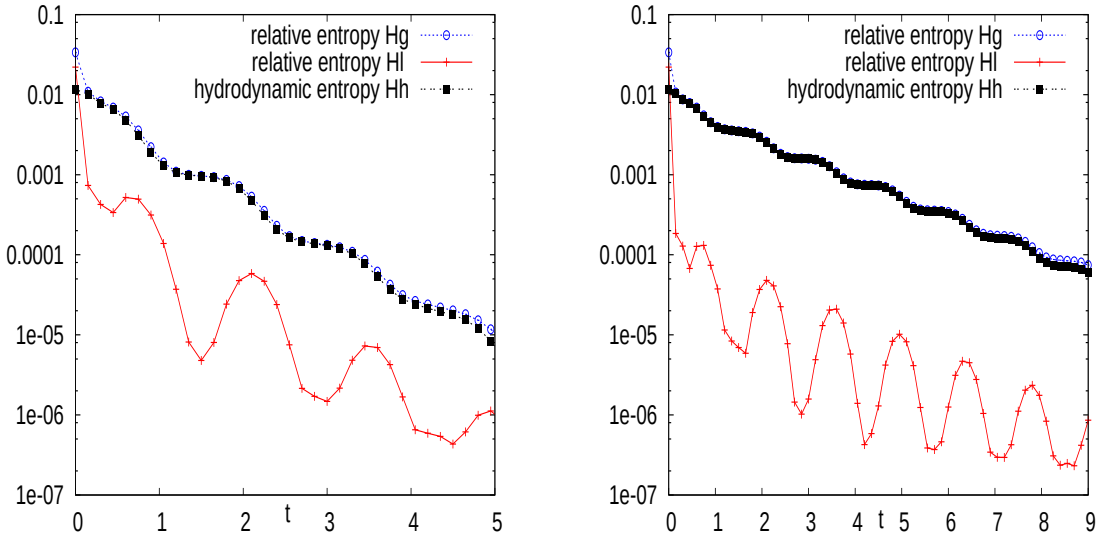

(1) $\varepsilon = 0.125$ (2) $\varepsilon = 0.05$

FIGURE 6. Trend to equilibrium: *time evolution of the entropy relative to the global equilibrium $\mathcal{H}_g$, entropy relative to the local equilibrium $\mathcal{H}_l$ and hydrodynamic entropy $\mathcal{H}_h$ (1) $\varepsilon = 0.125$ and (2) $\varepsilon = 0.05$ in log scale.*

5.5. **The ghost effect.** It has been shown analytically [35, 3] and numerically [36] on the basis of the kinetic theory that the heat-conduction equation is not suitable for describing the temperature field of a gas in the continuum limit in an infinite domain without flow at infinity, where the flow vanishes in this limit. Indeed, as the Knudsen number of the system approaches zero, the

temperature field obtained by the kinetic equation approaches that obtained by the asymptotic theory and not that of the heat-conduction equation, although the velocity of the gas vanishes. Here we review such a phenomenon, called the ghost effect, in the framework of the simulation of the Boltzmann equation.

We consider a gas between two plates at rest in a finite domain. In this situation, the stationary state at a uniform pressure (the velocity is equal to zero and the pressure is constant) is an obvious solution of the Navier-Stokes equations; the temperature field is determined by the heat conduction equation [35], which is given for $d_v = 2$ and Maxwell molecule kernel, $B(u, \cos\theta) = 1$, by

$$u = 0, \quad \rho T = C, \quad -\nabla_x \cdot (T \nabla_x T) = 0.$$

According to the Hilbert expansion with respect to the Knudsen number ε, the density and temperature fields in the continuum limit are affected by the velocity field, which is of order one with respect to ε. Finally, the heat conduction equation, although extracted from the incompressible Navier-Stokes system, is not appropriate in a whole class of situations, in particular when isothermal surfaces are not parallel, thereby giving rise to "ghost effects".

In this section, we will show that the numerical solution agrees with one obtained by the asymptotic theory and not with the one obtained from the heat conduction equation; this result is a confirmation of the validity of the asymptotic theory. This problem has been already studied from the numerical point of view for the time independent BGK operator, but not for the full time dependent Boltzmann equation for hard sphere molecules.

Consider a rarefied gas between two parallel plane walls at $y = 0$ and $y = 1$. Both walls have a common periodic temperature distribution T_w

$$T_w(x) = 1 - 0.5\,\cos(2\,\pi\,x); \quad \forall x \in (0, 1),$$

and a common small mean velocity u_w of order ε in its plane

$$u_w(x) = (\varepsilon, 0).$$

On the basis of kinetic theory, we numerically investigate the behavior of the gas, especially the temperature field, for various small Knudsen numbers ε. Then, we will assume:

- the behavior of the gas is described by the Boltzmann equation for hard sphere molecules.
- the gas molecules make diffuse reflection on the walls (complete accommodation).
- the solution is 1-periodic with respect to x. Then, the average of pressure gradient in the x direction is zero.

In this example, the walls are moving with a speed of order ε. We apply the deterministic scheme in $2d_x \times 2d_v$ and choose a computational domain $[-7, 7] \times [-7, 7]$ in the velocity space with a number grid points $n = 32$ in each direction, $M = 4$ and for the space direction $n_x = n_y = 50$. Finally we take $\Delta t = 0.001$.

The isothermal lines and the velocity field for $\varepsilon = 0.02$ are shown in Figure 8. These results are in good agreement with those obtained by discretizing the the BGK operator [35]. Moreover, according to the numerical simulations presented in [35], the temperature field deviates from one given by the heat conduction equation and is increasing when the Knudsen number ε goes to zero whereas the velocity flow is vanishing (Figure 7).

The temperature converges to the temperature given by the Asymptotic theory developed by Sone *et al.* [35] and not to the solution of the Heat equation. Let us note that in this particular case, we cannot compute an accurate solution for very small Knudsen number, because the computational time to reach the stationary solution with a very good accuracy becomes too large.

Finally, we also present the time evolution of the entropy $H(f)$ with respect to the final state H_∞ in order to investigate the rate of convergence to equilibrium. Clearly, this result illustrate that the boundary effects does affect the rate of convergence, which is strongly influenced by the Knudsen number ε. In Table 1, we report the rate of convergence obtained from the numerical results with

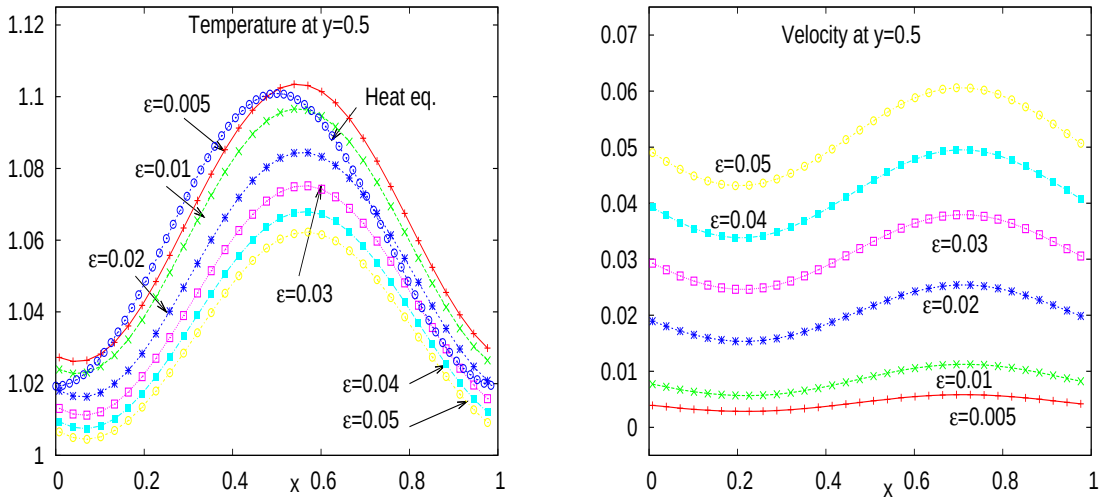

(1) (2)

FIGURE 7. Ghost effect: *temperature and mean velocity along $y = const$ for various Knudsen numbers $\varepsilon = 0.01$, 0.02, 0.03, 0.04 and 0.05, (1) temperature at $y = 0.5$ (2) mean velocity u at $y = 0.5$.*

ε	rate of convergence α	ratio α/ε
0.050	0.52	10.40
0.040	0.42	10.50
0.030	0.32	10.66
0.020	0.225	11.25
0.010	0.123	12.30
0.005	0.066	13.20

TABLE 1. Ghost effect: *Influence of the Knudsen number on the damping rate for $\varepsilon = 0.005$ to 0.05.*

respect to ε. From these computations, the rate of convergence is clearly related to the Knudsen number, but we cannot really conclude that it is only proportional to ε. Let us emphasize that from our deterministic method we are able to compute the correct stationary state of the kinetic equation, but also the time evolution of macroscopic quantities and entropy.

Let us mention that the qualitative behavior of the stationary solution is close to the one obtained in [35, 3]. Of course since here we only consider $2d_v$ for Maxwell molecules whereas the numerical simulation presented in [35, 3] considered $3d_v$ BGK equation, isothermal lines and the amplitude of flow differs and is smaller in our case.

6. Conclusions

In this paper we present an accurate deterministic method for the numerical approximation of the space non homogeneous, time dependent Boltzmann equation in a bonded domain with different boundary conditions. The method couples a second order finite volume scheme for the treatment of the transport step with a Fourier spectral method for the collision step. It possesses a high order of accuracy for this kind of problems. In fact it is second order accurate in space, and spectrally accurate in velocity. The high accuracy is evident from the quality of the numerical results that

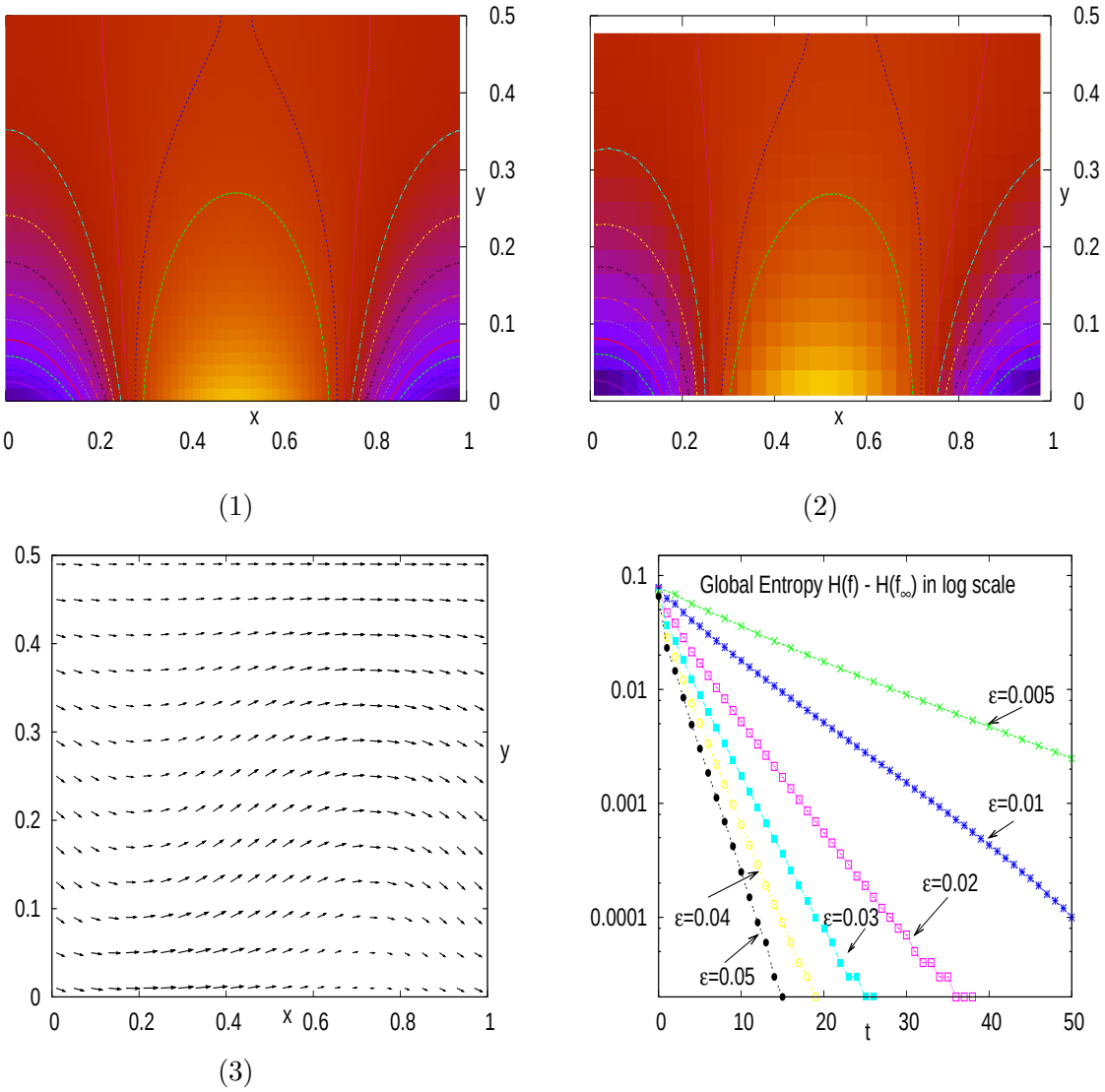

FIGURE 8. Ghost effect: *(1) isothermal lines for the numerical solution to the heat equation, (2) isothermal lines (3) and mean velocity u for a fixed Knudsen number $\varepsilon = 0.01$ (4) Evolution of the entropy $H(f) - H_\infty$ in* log *scale.*

can be obtained with a relatively small number of grid points in velocity domain. An effective time discretization allows the treatment of problems with a considerable range of mean free path, and the decoupling between the transport and the collision step makes it possible the use of parallel algorithms, which become competitive with state-of-the-art numerical methods for the Boltzmann equation.

The numerical results, and the comparison with other numerical results available in the literature, show the effectiveness of the present method for a wide class of problems. These results illustrate the accuracy and the interest of such a method for low Mach number flows or/and low Knudsen number for which boundary layer may occur. The main inerest concerns application to micro-channels.

Acknowledgment

The author would like to acknowledge the many valuable suggestions made by Irene Gamba on the application of Spectral methods for discontinuous solutions and Kazuo Aoki on the ghost effect.

References

[1] G. A. Bird, Molecular gas dynamics. *Clarendon Press, Oxford* (1994).
[2] A. V. Bobylev, The theory of the nonlinear spatially uniform Boltzmann equation for Maxwell molecules. *Math. Phys. Reviews*, vol. **7**, pp. 111–233 (1988).
[3] A. V. Bobylev, Quasistationary hydrodynamics for the Boltzmann equation, *J. Stat. Phys.* **80**, (1995).
[4] A. V. Bobylev and S. Rjasanow, Difference scheme for the Boltzmann equation based on the fast Fourier transform. *European J. Mech. B Fluids* **16**, pp. 293–306 (1997).
[5] A. V. Bobylev and S. Rjasanow, Fast deterministic method of solving the Boltzmann equation for hard spheres *Eur. J. Mech. B Fluids* **18**, pp. 869–887 (1999).
[6] C. Canuto, M. Y. Hussaini, A. Quarteroni and T. A. Zang, Spectral methods in fluid dynamics. *Springer Series in Computational Physics, Springer-Verlag, New York*, (1988).
[7] T. Carleman, Sur la théorie de l'équation intégrodifférentielle de Boltzmann, *Acta Math.* **60** (1932).
[8] C. Cercignani, The Boltzmann equation and its applications. *Springer-Verlag, Berlin* (1988).
[9] C. Cercignani, R. Illner and M. Pulvirenti, The Mathematical Theory of Dilute Gases. *Appl. Math. Sci.* **106**, Springer-Verlag, New York, (1994).
[10] P. Degond, L. Pareschi and G. Russo, Modeling and Computational Methods for Kinetic Equations. Series: Modeling and Simulation in Science, Engineering and Technology, Birkhäuser (2004).
[11] L. Desvillettes and C. Villani, On the trend to global equilibrium for spatially inhomogeneous kinetic systems: the Boltzmann equation. *Invent. Math.* **159**, pp. 245–316 (2004).
[12] G. Dimarco and L. Pareschi, Exponential Runge-Kutta methods for stiff kinetic equations. preprint
[13] R. S. Ellis and M. A. Pinsky, The first and second fluid approximations to the linearized Boltzmann equation. *J. Math. Pures et Appl.* **54**, pp. 125–156 (1975).
[14] F. Filbet, E. Sonnendrücker and P. Bertrand, *Conservative Numerical schemes for the Vlasov equation*, J. Comput. Phys. **172** (2001), 166-187.
[15] F. Filbet and L. Pareschi, A numerical method for the accurate solution of the Fokker-Planck-Landau equation in the non homogeneous case. *J. Comput. Phys.* **179**, pp. 1–26 (2002).
[16] F. Filbet and G. Russo, High order numerical methods for the space non-homogeneous Boltzmann equation. *J. Comput. Phys.* **186**, pp. 457–480 (2003).
[17] F. Filbet, L. Pareschi and G. Toscani, Accurate numerical methods for the collisional motion of (heated) granular flows. *J. Comput. Phys.* **202**, pp. 216–235 (2005).
[18] F. Filbet, C. Mouhot and L. Pareschi, Solving the Boltzmann equation in $N \log_2 N$. *SIAM J. Sci. Comput.* **28**, (2006) pp. 1029–1053
[19] F. Filbet and G. Russo Accurate numerical methods for the Boltzmann equation. *Modeling and Computational Methods for Kinetic Equations. Model Sumil. Sci Eng. Technol. Birkäuser Boston*, pp. 117–145 (2004).
[20] F. Filbet and S. Jin, A class of asymptotic preserving schemes for kinetic equations and related problems with stiff sources, *J. Comput. Phys.* **229** (2010), no. 20.
[21] I. Gamba and S. H. Tharkabhushanam, Spectral-Lagrangian methods for collisional models of non-equilibrium statistical states. *J. Comput. Phys.* **228** (2009), no. 6, 20122036.
[22] I. Gamba and S. H. Tharkabhushanam, Shock and boundary structure formation by spectral-Lagrangian methods for the inhomogeneous Boltzmann transport equation. *J. Comput. Math.* **28** (2010), no. 4, 430460.
[23] T. Ohwada, Investigation of heat transfer problem of a rarefied gas between parallel plates with different temperatures, *Rarefied gas dynamics, ed. C. Shen, Peking University*, pp. 217-234
[24] I. Ibragimov and S. Rjasanow, Numerical solution of the Boltzmann equation on the uniform grid. *Computing* **69** (2), pp. 163–186 (2002).
[25] J. C. Maxwell, *Philos. Trans. R. Soc. London* **70**, 231 (1867).
[26] C. Mouhot and L. Pareschi, Fast algorithms for computing the Boltzmann collision operator. *Math. Comp.*
[27] G. Naldi, L. Pareschi and G. Toscani, Spectral methods for one-dimensional kinetic models of granular flows and numerical quasi elastic limit. *ESAIM RAIRO Math. Model. Numer. Anal.* **37**, pp. 73–90 (2003).
[28] K. Nanbu, Direct simulation scheme derived from the Boltzmann equation. I. Monocomponent Gases. *J. Phys. Soc. Japan* **52**, pp. 2042–2049 (1983).
[29] L. Pareschi, Second order fast conservative schemes for the ergodic approximation of general Boltzmann equations. In preparation.

[30] L. Pareschi and B. Perthame, A Fourier spectral method for homogeneous Boltzmann equations. *Trans. Theo. Stat. Phys.* **25**, pp. 369–382 (1996).
[31] L. Pareschi and G. Russo, Numerical solution of the Boltzmann equation I. Spectrally accurate approximation of the collision operator. *SIAM J. Numer. Anal.* **37**, pp. 1217–1245 (2000).
[32] L. Pareschi, G. Russo and G. Toscani, Fast spectral methods for the Fokker-Planck-Landau collision operator. *J. Comput. Phys.* **165**, pp. 216–236 (2000).
[33] L. Pareschi and G. Russo, On the stability of spectral methods for the homogeneous Boltzmann equation. *Trans. Theo. Stat. Phys.* **29**, pp. 431–447 (2000).
[34] D.J. Rader, M.A. Gallis, J.R. Torczynski and W. Wagner, Direct simulation Monte Carlo convergence behavior of the hard-sphere-gas thermal conductivity for Fourier heat flow *Phys. Fluids* 18, 077102 (2006)
[35] Y. Sone and M. Wakabayashi, Flow induced by nonlinear thermal stress in a rarefied gas, *Proceedings of Symposium on Mechanics of Space Flight Institute of Space Sciences*, Tokyo, 1988, p. 14 (in Japanese).
[36] Y. Sone, K. Aoki, S. Takata, H. Sugimoto and A.V. Bobylev, Inappropriateness of the heat-conduction equation for description of a temperature field of a stationary gas in the continuum limit: examination by asymptotic analysis and numerical computation of the Boltzmann equation. *Phys. Fluids* **8** (1996), 628–638.
[37] R. Strain and Y. Guo, Almost exponential decay near Maxwellian. To appear in *Comm. Partial Differential Equations*.
[38] M. Tij, M. Sabbane, and A. Santos, Phys. Fluids 10, 1021 (1998).
[39] F. J. Uribe and A. L. Garcia, Burnett description for plane Poiseuille flow, *Phys. Rev. E* **60**, 4063 (1999).
[40] C. Villani, A survey of mathematical topics in kinetic theory. *Handbook of fluid mechanics*, S. Friedlander and D. Serre, Eds. Elsevier Publ., (2002).

Francis Filbet

Université de Lyon,
Institut Camille Jordan, CNRS-UMR 5208
Université Claude Bernard, Lyon 1
43 boulevard 11 novembre 1918,
F-69622 Villeurbanne cedex, FRANCE

e-mail: filbet@math.univ-lyon1.fr